



ISSN: 2321-2152

IJMECE

*International Journal of modern
electronics and communication engineering*

E-Mail

editor.ijmece@gmail.com

editor@ijmece.com

www.ijmece.com

Next-Gen Three-Phase Multiport DC-AC Inverter for Enhanced Photovoltaic and Storage System Efficiency

¹Talari Manohar, ²Talari Geethambika, ³Agrahara Surya Narayana Reddy, ⁴P Asifulla, ⁵Somande Palli Karanam Harshith, ⁶Puppala Harini,

¹Assistant Professor, Department Of EEE, Ananthalakshmi Institute Of Technology And Sciences, Itikalapalli, Near Sk University, Ananthapur.

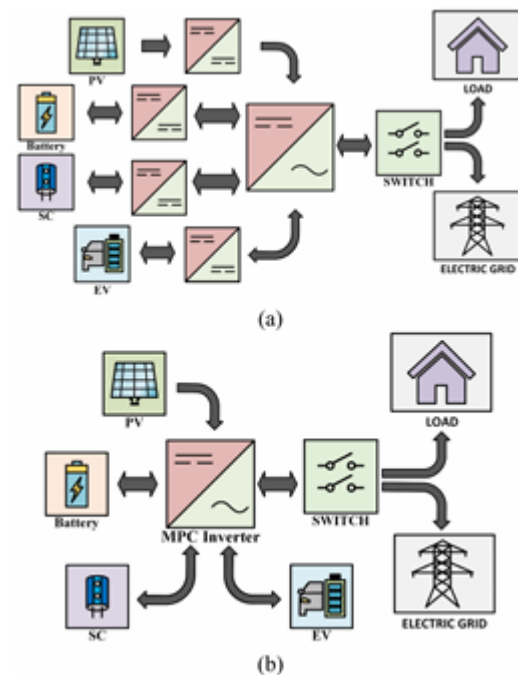
^{2,3,4,5,6} Student, Department Of EEE, Ananthalakshmi Institute Of Technology And Sciences, Itikalapalli, Near Sk University, Ananthapur.

Abstract

Distributed renewable energy sources paired with hybrid energy storage systems enable the smoothing of electric power supply as well as the provision of auxiliary services to the electric grid. In these applications, complicated and costly topologies using many independent dc-dc and dc-ac converters are used. A new non-isolated multiport dc-ac power converter with reduced passive components and high-frequency power semiconductor use is presented in this article. The suggested grid-connected multiport converter (MPC) enables the integrated power management of electrolytic battery units, photovoltaic (PV) arrays, super capacitor banks, and electric vehicle (EV) battery packs. To enable bidirectional power flow and direct connection of the PV source to the dc link, the proposed MPC inverter's power circuit employs a unique variation of the split-source inverter design. The proposed design is accompanied by a specifically engineered control method that enables the maximum power point tracking process to be executed without an extra power converter, the power flow at each port to be independently regulated, and the power flow between its ports to be managed. We have constructed a working model of the proposed MPC inverter and verified its operation under various power flow conditions.

Index Terms—Bidirectional power flow, dc-ac inverter, electric grid, energystorage(ES), multiportconverter(MPC), photovoltaic (PV) array.

including wind turbines and photovoltaic (PV) arrays. This is in response to growing energy and environmental concerns. The primary issue with these RESs, however, is that their energy output is not constant since it is affected by weather conditions that change over time [1, 2]. Hybrid energy storage (ES) systems, which combine various storage technologies like battery banks, are designed to address this issue.



INTRODUCTION

A growing number of people are considering using power generation from renewable resources,

Fig. 1. Topologies for the interconnection of multiple energy production and storage units.

By making use of a series of separate power converters. part (b) Integrating the electric power supply, meeting the demands of dynamic loads, and providing supplementary services to the electric grid, such as P-Q regulation and frequency control, are all achieved via a design that combines multi-phase current (MPC) with supercapacitors (SCs) [3]. Concurrently, a substantial amount of research has concentrated on EVs and their potential use as distributed ES units [4, 5]. The integrated RES-ES-EV-load/grid system requires a number of dc-dc and dc-ac converters to regulate the power flow between the sources, as shown in Figure 1(a) [6, 7, 8]. This approach results in inefficient regulation of power flow and makes the system design more complicated. To overcome these constraints, scientists have developed multiport power converters (MPCs), as shown in Figure 1(b), which combine many converters into one. With an MPC, you get more bang for your buck, less control stages, less components, and a smaller footprint [9]. For the purpose of combining RESs and ES systems to provide power for either loads or the grid, many dc-dc MPC topologies have been proposed so far (e.g., [10]). To connect these MPC converters to the utility grid, nevertheless, an additional dc-ac inverter is required. By using a two-stage single-phase dc ac converter, an ac microgrid may be linked to a PV source, a wind turbine, and batteries, as shown in [11]. This isolated MPC converter is inefficient, heavy, and expensive due to the two transformers that are necessary to construct it. It is proposed in [12] to use an isolated single-phase dc-ac converter to control the flow of power among RESs, EVs, and the power grid. This method increases the number of power switches by using a multitude of individual power converters. But in the end, nonisolated dc-ac MPC topologies are more cost-effective, compact, and manageable than isolated ones. Two direct current inputs and one or three phase alternating current outputs characterize the three-port bidirectional nonisolated converter proposed in [13]. The experiments made use of a battery and a capacitor as their direct current inputs. This article [14] details the steps necessary to construct a three-phase dc-ac converter for use in PV power plants. The design allows for the deployment of a maximum power point tracking (MPPT) mechanism in separate PV strings via the use of independent dc-dc converters linked to each string input port. The grid connection is made possible by the employment of a three-phase full-bridge dc-ac inverter. In [15], the

authors detail a bidirectional ac-dc rectifier that may be used for ES purposes. They have a capacitor connected to the dc bus and a bank of batteries attached to the dc input port. It takes a lot of power switches with this design to make a single-phase grid work for bidirectional power flow. The dc-ac split-source inverter (SSI) shown in [16] consists of a dc source, a dc-link capacitor port, and a three-phase ac output. A three-phase bridge uses three diodes to connect each leg to the dc port's inductor.

One parameter controls the ac and dc power flows via the SSI. According to [17], a control approach including two control variables may be used to separately govern the dc and ac sides. In [18], an SSI with a single-stage, single-phase design is detailed, along with its DC supply and DC-link capacitor port. One leg of the full-bridge power stage must charge an inductor at a constant duty cycle while the other leg uses sinusoidal pulsewidth modulation (PWM) to generate a voltage for a single-phase alternating current (ac). Each leg of the full-bridge stage is connected to a power switch that operates at fundamental frequency. The present dc-ac MPC topologies have the following shortcomings when it comes to connecting different energy production and storage devices to the power grid: To start with, you won't find many of them with a three-phase ac output. Secondly, the dc input ports don't support bidirectional power flow, so you can't connect many different types of dc power sources. For instance, you can't use a unidirectional port to recharge a battery or SC. To meet this need, a new nonisolated three-phase multiport dc-ac inverter is presented in this paper. Unlike previous works that have combined a conventional three-phase full-bridge converter with numerous dc-dc converters connected to a shared dc bus, this article proposes a multilevel dc/ac converter that connects the PV source straight to the dc link, thus obviating the need for a separate power converter [6, 7, and 8]. Furthermore, a new method of control has been developed to achieve the same objective, and the research of Lee and Heng [18] is first applied to a three-phase SSI power circuit in the present literature to permit bidirectional power flow. The suggested MPC inverter uses a combined power circuit and control approach to regulate the flow of power across four independent dc input ports. Power conversion to and from the grid, as well as connections with PV arrays, EV batteries, battery banks, and SCs, are all possible via these ports. Table I contains the recommended MPC inverter topology and all of the related topologies that have been offered before. In comparison to previous studies, this article proposes the following novel aspects of the MPC inverter. 1) The suggested MPC inverter

includes five input ports, which is the greatest number among existing three-phase MPC topologies. These include four independent dc ports and one three-phase ac port. Second, across four of the five ports, current may go either way. 3) The proposed control method enables the concurrent execution of an MPPT process, and the PV source is directly connected to the dc connection. Figure 1(a) shows a design that employs separate dc-dc and dc-ac converters for each input/output port; the proposed topology reduces the number of high-frequency power semiconductors and passive components. As a result, the whole power processing system becomes more reliable and costs less.

. 5). The decoupled closed-loop control approach is an integral part of the proposed MPC inverter design. It allows for independent regulation of each port's power flow and management of the power flow between the various ports of the inverter. 6) This is the first instance of a three-phase SSI with bidirectional power flow and various power sources linked to the dc-link capacitor that has been published in the current literature. In this paper, the

experimental findings are reported, demonstrating that the suggested MPC inverter successfully operates under different power flow situation. What follows is an outline of the remaining content of this piece. In Section II, we provide a comprehensive review of the topology that was put into place. In Section III, we examine the suggested method of control. The outcomes of the experiments are detailed in Section IV. Lastly, this essay is concluded in Section V.

PROPOSED MPC INVERTER

Instead of employing separate dc-dc and dc-acconverters for each input and output port, an MPCinverter is proposed in this article. The structure's total complexity, cost, and component count might be reduced using this. The proposed design is shown in Figure 2. It includes a three-phase alternating current load or electric grid that may be connected to no more than four separate direct current sources, one of which is a photovoltaic array.

TABLE I COMPARISON OF MULTIPOINT DC-AC INVERTER TOPOLOGIES

Topology	Comparison Parameters					AC output
	Number of inductors (AC output filter not included)	Number of capacitors (AC output filter not included)	Number of power switches	Number of power diodes	Number of DC input ports	
Proposed in this article	3	4	10 high-frequency and 3 low-frequency	10 high-frequency and low-frequency	4	Three-phase
With separate dc-dc and dc-dc converters for four dc ports (e.g. based on the article presented in [6])	4	8	13 high-frequency	13 high-frequency	4	Three-phase
PV-wind-battery isolated MPC [11]	1 + 2 transformers	3	8	12	3	Single-phase
RES-EVs isolated MPC with individual dc-dc converters [12]	6 + 1 transformer	3	26	28	6	Single-phase
Bidirectional nonisolated three-port MPC [13]	3	0	6	6	2	Three-phase
Single-stage MPC with separate DC-DC converters at each PV string input port [14]	2	2	8	16	2	Three-phase
Bidirectional AC-DC rectifier for ES with dc-bus capacitor [15]	1	1	10	10	2	Single-phase
DC-AC SSI with DC source and DC-link capacitor [16]	1	1	6	9	2	Three-phase
Single-phase/single-stage SSI with DC source and DC-link capacitor [18]	1	1	6	6	2	Single-phase

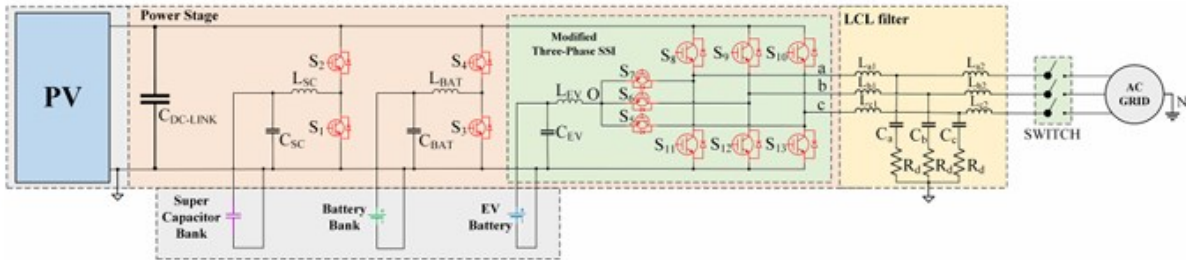


Fig. 2. Circuit diagram of the proposed three-phase MPC inverter.

in order to control the flow of power between various components, such as EV batteries, SC banks, and batteries. The connecting diodes and S5, S6, and S7 all function at a low frequency of 50Hz. The PV array is directly connected to the dc connection, which reduces the total number of passive components and semiconductor switches. As we'll see later on, this opens the door to the option of doing an MPPT process. Power Circuit Architecture (A) Figure 2 shows that the suggested MPC inverter has one ac port and four dc ports. The dc ports allow for the connection of various components, including the PV array, SC, electronic vehicle batteries, and battery banks. You may connect the ac side to electric loads or the grid. A direct connection between the PV array and the DC-link capacitor (CDC-link) is established. The suggested MPC inverter's control unit continuously alters the dc-link voltage to implement the MPPT process, which will be discussed later on. The battery and the SC are connected to the dc link using bidirectional power circuits. The suggested MPC inverter has several input/output ports, thus it is important to handle the battery and SC connection circuits properly. This is essential because the MPPT process continuously controls the dc-link voltage. Each subcircuit receives its matching source as input from two insulated-gate bipolar transistor (IGBT) power switches with antiparallel diodes, enabling a two-way current flow. An example of a single-phase form of SSI is described in [18] as a full-bridge inverter that incorporates an inductor and a dc-link capacitor employing two power switches. The author extends the work of Lee and Heng [18] to a three-phase SSI by connecting the EV port inductor (LEV) to the switching nodes of a three-phase full-bridge inverter and making use of three fundamentally-frequency IGBT power switches (S5, S6, and S7 in Fig. 2). In Figure 1(a), it is shown that using a

separate dc-dc converter to link the EV to the dc connection will raise the overall cost and switching losses of the MPC inverter. A high-frequency power switch is required for this. Along with the suggested MPC inverter power circuit's aforementioned capabilities, this article also offers a novel control technique that may be used to achieve them. For the dc-dc conversion to work in a full-bridge inverter, one of the three legs must maintain a constant duty cycle. The second pair of legs operates at a much altered sinusoidal

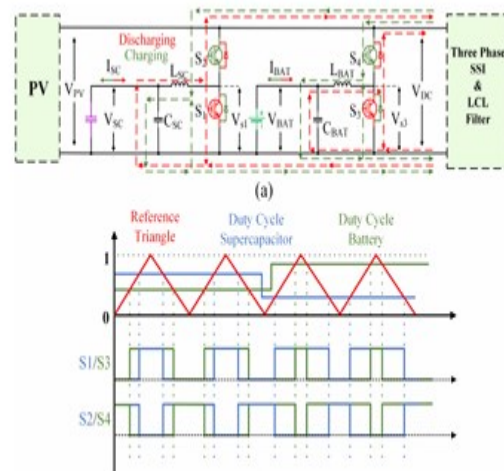


Fig. 3. (a) Alternative current flows of the battery and SC interconnection circuits of the proposed MPC inverter during a switching period. (b) Gate pulses for S1–S4, duty cycle for SC, and duty cycle for Battery.

By connecting the leg that operates at a constant duty cycle to the inductor and EVbatteryport, the dc-link voltage may be adjusted using the three basic frequency switches (S5, S6, and S7). As a result, the power flow of the proposed MPC inverter may be adjusted both globally and for each individual port. We will now discuss the basic idea and methods of control for the power switches. The Basic Concept and Indicators of Operation Part B Depending on the power balance among its ports, the proposed MPC inverter may support several alternate power flow situations, as shown by the arrows in Figure 1(b). During a switching phase, two current flows may occur, as seen in Figure 3(a): one from the battery, and another from the SC's charging and discharging modes. From States 1 to S4, the operational waveforms and gate signals are shown in Figure 3(b). A reference triangle signal with a frequency equal to the goal switching frequency of the MPC inverter is used to compare the constant (duty cycle) of each input source. The switch is placed to the off-state when the duty cycle is greater than the value of the triangle pulse; otherwise, it is put to the on-state. S1 and S3 are complementary switches that work well when used with S2 and S4. Each phase of the three-phase alternating current grid is represented by one of the three legs of the three-phase bridge. A bridge leg consists of two complementary pulse-receiving IGBTs that have diodes that are antiparallel to one another. Thus, S8 is an ideal complement to S11 in phase a, S9 and S12 in phase b, and S10 and S13 in phase c. Charging and discharging the lithium-ion battery in the electric car occurs in cycles that are controlled by the power switches. The two are connected in series. An inductor LEV is connected to three IGBTs in a full-bridge circuit via antiparallel diodes (S7, S6, and S5). With each leg (a, b, and c) linked to one of the transistors, the circuit operates as a bridge. This connection causes an interaction between the electric car battery and the control of the three-phase bridge circuit; moreover,

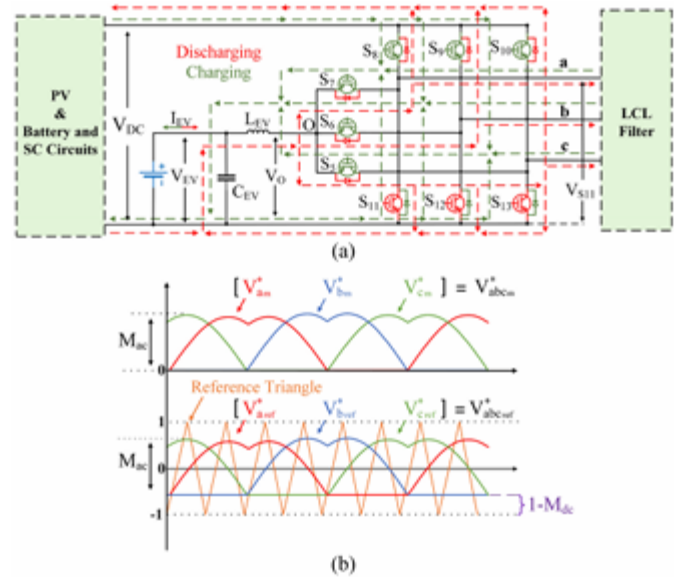


Fig. 4. Operation of the modified three-phase SSI subcircuit of the proposed MPC inverter. (a) Alternative current flows. (b) Reference signals analyzed in the following.

As shown in Figure 2 with the EV source, the alternate current flow via the redesigned three-phase SSI subcircuit of the proposed MPC inverter is shown in Figure 4(a). At first, the control unit of the proposed MPC inverter generates three symmetrical sinusoidal reference waves with a phase difference of 120° in order to provide suitable driving pulses for the integrated gate bipolar transistors (IGBTs) in the full-bridge circuit and the electric vehicle battery. As shown in Figure 4(b), the reference signals are created by modifying the three sinusoidal waves according to the steps outlined in Section III. In terms of reference signal amplitude, we have the ac modulation index M_{ac} , and in terms of reference signal offset, we have the dc modulation index M_{dc} . To accomplish the target power flow, the values of M_{ac} and M_{dc} are tuned. In order to produce the S7, S6, and S5 driving pulses, the EV's reference signal is compared to zero. We turn on the associated power switch when its reference signal is zero and turn it off otherwise. Figure 5(a) shows the process. When the reference signal for each leg of the whole bridge is larger than or equal to the width of the triangle pulse, then the associated switch is turned ON to create driving pulses for the three-phase bridge switches; otherwise, it is turned OFF [see Fig. 5(b)]. For example, switches S11, S12, and S13 work well with switches S8, S9, and S10, respectively. The reference signals used to operate the three EV switches have a

phase difference of 120° , as previously stated. Therefore, a separate switch is turned off at 120° (during the charging cycle). Each time the battery is charged, one leg of the bridge converts the direct current (dc) from the link voltage to direct current (dc) while the other two legs convert the dc to alternating current (ac). The three-phase bridge's connection to S7 acts as a dc-dc converter while the other two legs regulate the dc-ac inversion, as seen in Figure 6(a) when S7 is ON and S6 and S5 are OFF. The other two power switches are similarly handled.

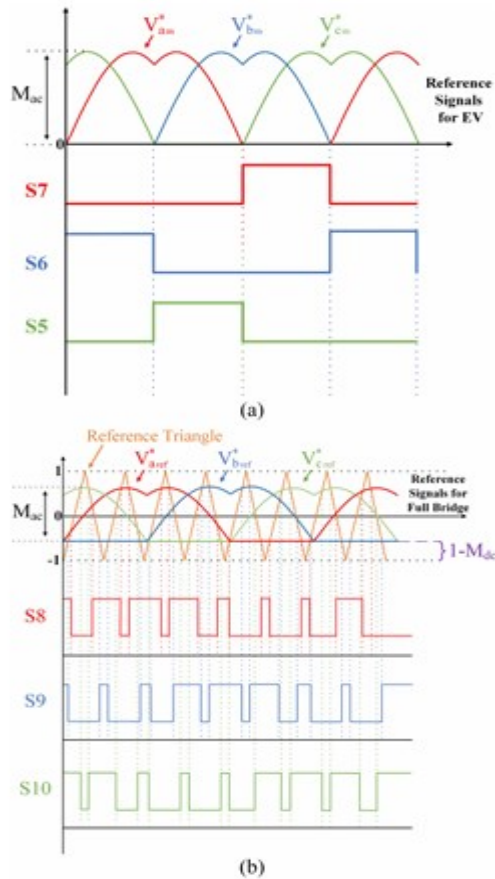


Fig. 5. Gate pulses for (a) EV port switches and (b) full-bridge switches.

The three separate power switches on the EV port are receiving a constant current, which is then used to charge the SSI subcircuit's EV port (see to Fig. 7). The SSI subcircuit's potential switching state combinations are shown in Table II, with "1" and "0" denoting the related switch's ON and OFF states, respectively. It is important to additionally take into account the EV battery switches (S7, S6, and S5) due to the connection of the SSI port. Every cycle has three possible states—100, 010, and 001—that may be achieved by activating only one of the three

switches. All eight states of the complete bridge may be mixed with these three, for a grand total of twenty-four states. Table II shows that out of all these states, only 15 are legitimate; the other 9 are not viable. The reference signal for a full-bridge leg must be equal to 1 minus M_{dc} before the EV switch linked to that leg may be switched ON. The high-side switch of the leg that operates at a constant duty cycle is turned off when the difference triangle is more than $1 - M_{dc}$ and less than the maximum value of the modulating signals (V_{Δ}^{abcref}), as illustrated in Figure 5. The reference triangle must be smaller than $1 - M_{dc}$ for that leg's switch to be turned ON. If the values of the modulating signals from the other two high-side switches are larger than the difference triangle, then all three of them are switched on. This is because the only way for a high-side switch to operate at a constant duty cycle is

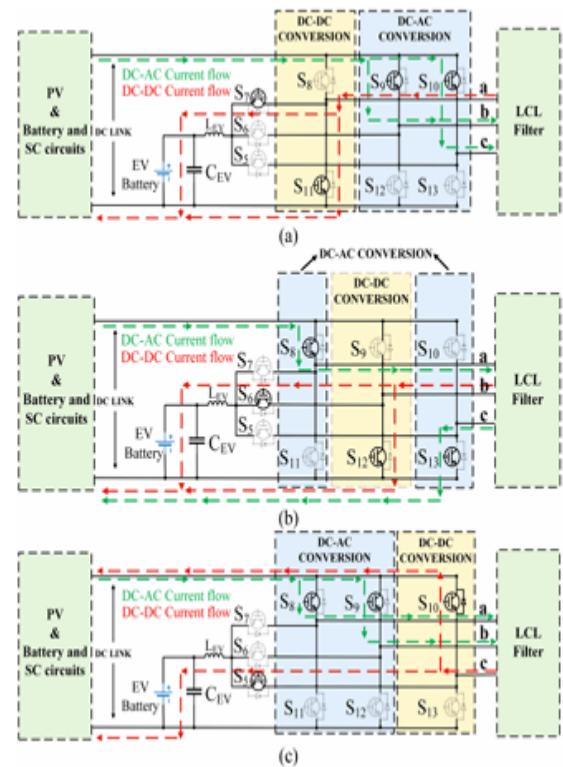


Fig. 6. Alternative switching states of the modified three-phase SSI subcircuit of the proposed MPC inverter during charging. (a) State 5. (b) State 9. (c) State 24.

PROPOSED CONTROL SCHEME

First, there's the unit, which controls the power going into the MPC inverter from the battery and SC.

Finally, the PV MPPT controller maintains a constant dc-link voltage in accordance with the PV MPPT algorithm. Third, the redesigned three-phase SSI subcircuit controller adjusts the values of M_{dc} and M_{ac} , respectively, to regulate the current flowing into the EV port and the current going out of the inverter. Part A: Managing the Motor and the Battery In Figure 8, can see the battery and SC current controllers in action. The detected values from each source are compared with the converted values of the needed power setpoints (P_{BAT}^* , P_{SC}^*) using current reference values (I_{BAT}^* , I_{SC}^*). The next step is to use the error to tell a PI controller to generate the appropriate duty cycle value. Two complimentary pulse width modulation (PWM) signals, one for each duty cycle (refer to Figures 2 and 3), might be used to operate the (S1, S2, S3, and S4) switches of the proposed MPC inverter.

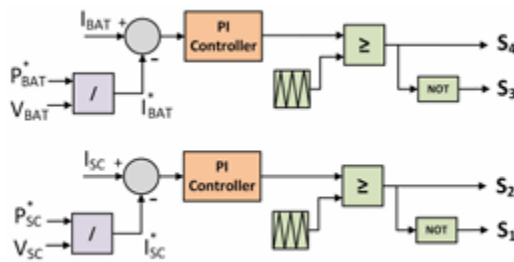


Fig. 8. Battery and SC current control loops.

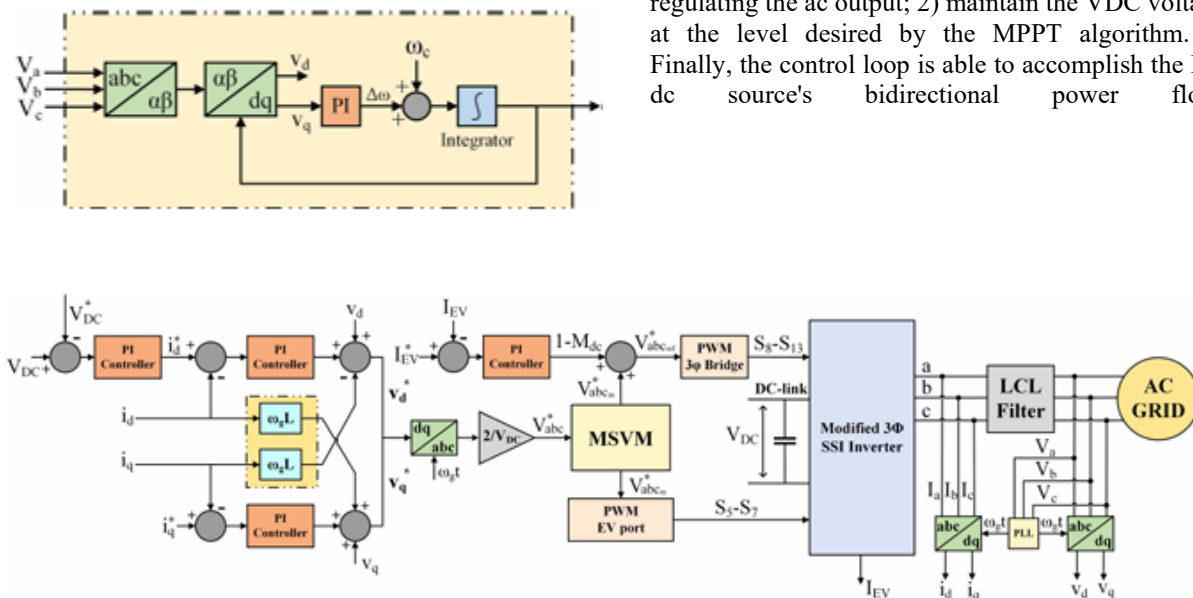


Fig. 9. SRF-PLL block diagram.

Figure 8 shows that the proposed controller charges and discharges the battery and SC banks by modifying the P_{BAT}^* and P_{SC}^* power setpoints. B. PVArray MPPT Control Loop Figures 3 and 4 show the direct regulation of the dc-link voltage, or VDC, to control the PV array's power output. In order to conduct the PVMPPT process, which yields the voltage level (V_{DC}^* in Fig. 10) that corresponds to the maximum power of the PV array, the perturbation and observation approach [19] is used. The output current controller (i_d in Fig. 10) employs a modified synchronous reference frame control technique—to be described later on—to regulate the inverter's power output. As a result, the whole PV power is produced and the dc-link voltage stays at the MPPT setpoint V_{DC}^* . C. Motor Control for EVPort and Output Current Figure 2 shows the three-phase SSI subcircuit of the proposed MPC inverter, which includes the EVdc input and the three-phase full bridge connected to the ac grid. In spite of this, the modulation systems proposed in [16] merge the dc and ac SSI control parameters into a single number, the modulation index. A control strategy that integrates the synchronous reference frame method with the modulation outlined in [16] may be used to isolate the ac and dc components. Using this technique, the SSI may be operated in grid-connected mode with its dc and ac sides regulated independently. Changing the M_{dc} regulation index allows the control loop shown above to achieve the following: 1) manage the PV power output while regulating the ac output; 2) maintain the VDC voltage at the level desired by the MPPT algorithm. 3. Finally, the control loop is able to accomplish the EV dc source's bidirectional power flow.

Fig. 10. Control scheme of the PV array and the grid-connected

altered space-vector modulation approach and synchronous reference frame method comprise the suggested MPC inverter's SSI subcircuit. This article proposes an enhanced version of the synchronous reference frame control method first presented in [17] to achieve that goal. By converting the a-b-c grid voltages and currents into the d-q frame, which spins in sync with the electric grid voltage's angular frequency, synchronous reference frame control (also known as d-q control) is achieved.

$$G_{PI}^{(dq)}(s) = \begin{bmatrix} K_{p,d} + \frac{K_{i,d}}{s} & 0 \\ 0 & K_{p,q} + \frac{K_{i,q}}{s} \end{bmatrix} \quad (1)$$

$$v_d^* = \left(K_p + \frac{K_i}{s} \right) (i_d^* - i_d) - \omega_g L i_q + v_d \quad (2)$$

$$v_q^* = \left(K_p + \frac{K_i}{s} \right) (i_q^* - i_q) + \omega_g L i_d + v_q \quad (3)$$

A PI controller may effectively and rapidly regulate sinusoidal values transformed to dc signals by eliminating steady-state faults in this system. An MPC inverter based on the PI controller's d-q transfer function matrix is proposed in [20]. According to (1), the total of the controller's proportional gain ($K_{p,d(q)}$) and integral gain ($K_{i,d(q)}$) is equal to the generalized integral of the current along the d(q)-axis, $G(dq)$. Diagrams of the PV array and the modified SSI subcircuit meant to control it are shown in Figure 10, continuing from Figure 2. The dc-link voltage is controlled by the MPPT voltage in this configuration. Input errors to a PI controller are used to produce the active current reference (i_{d}^*), while the reactive current reference (i_{q}^*) is set to zero. The inverter output reference voltages (v_{d}^* and v_{q}^*) are calculated using the following equations in the d-q frame: One possible translation of the equation $v_{\phi d} = K_p + K_i s (i_{d}^* - i_d)$ is: $(-\omega_g L i_q + v_d)$. The equation is $v_{\phi q} = K_p + K_i s (i_{q}^* - i_q) + \omega_g L i_d + v_q$ (2) (3), where v_d and v_q are the measured grid voltages converted into the synchronous reference frame. After that, we get the sinusoidal reference values by translating the reference voltages into the natural ABC context. The signals cannot be compared to PWM signals produced by a triangular saw tooth carrier with values

ranging from -1 to 1, since these values instead span from $-V_{DC}/2$ to $V_{DC}/2$. Thus, as can be shown in Figure 10, the signals must be divided by $V_{DC}/2$ to provide an appropriate comparison. V_{abc}^* will be the values that result from this.

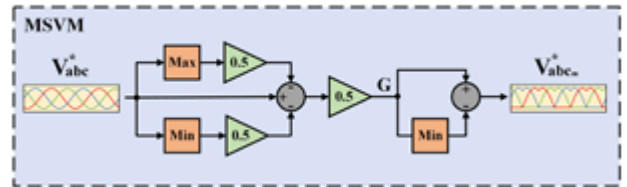


Fig. 11. Formation of MSVM reference signals from the synchronous reference frame block diagram.

Part E: Advanced Space-Vector Modulation (MSVM) An MSVM approach is combined with the previously revealed synchronous rotating frame control in [16]. The V_{abc}^* signals generated by the d-q controller are used to generate the MSVM signals, which are shown as V_{abc}^* in Figure 11. The MSVM proposed in reference [17] states that the minimum envelop of the modulating signals, $V_{\phi abc}$, should be kept at $1 - M_{dc}$. By allowing for the independent regulation of the audio output and the SSI subcircuit input, this adds an extra layer of control. To be more precise, the ac side is controlled by the modulation index M_{ac} , while the dc side (i.e., the EV source) is controlled by the regulation index M_{dc} . The error is then delivered to a PI controller after Fig. 2 illustrates the comparison between the reference value (I_{EV}^*) and the current of the EV battery input (I_{EV}) linked to the modified SSI subcircuit dc input (V_{EV}). Based on the current reference from the EV port, the PI controller modifies the M_{dc} parameter to regulate the negative envelope that was previously discussed. Be mindful that M_{dc} must be larger than M_{ac} in order to prevent the ac-side harmonic distortion from escalating. The dc-link voltage (V_{DC}) is connected to the EV port voltage (V_{EV}), as mentioned in [17].

$$V_{DC} = \frac{1}{1 - M_{dc}} \cdot V_{EV} \quad (10)$$

Furthermore, the following is the expression for the amplitude of the electric grid phase voltage ($V_{\phi 1,p}$) as a function of the dc-link voltage and modulation index:

$$V_{DC}^* \geq \left(V_{EV} + \sqrt{3} \cdot V_{\phi 1,pmax} \right) \quad (12)$$

$V_{\phi 1,pmax}$ stands for the greatest amplitude, or worst-case scenario, of the electric grid's phase voltage. Direct connection to the dc connection means that the voltage at the highest power point of the PV source must be higher than the minimum permissible voltage, as calculated from (12). Finally, the bridge pulses are generated using the modulating signals $V_{\phi 1,p}$, which are constructed using MSVM modulation with a M_{dc} offset added (see Fig. 4(b)).

F. Controlling the Port Switches for Electric Vehicles

This article proposes a modified SSI subcircuit of the MPC inverter that differs from the typical SSI in references [16] and [17]. Power switches have been used in place of the three diodes that linked the dc input to the inverter full bridge. Thus, current flows across the antiparallel diodes of the power switches, just like a typical SSI, while the electric vehicle's battery is being depleted. This is achieved by means of the modified SSI that is housed in the proposed MPC inverter. Conversely, when the EV battery is charged, switches S5, S6, and S7 are turned on sequentially using a 50 Hz phase difference. The reference signals ($V_{\phi 1,p}$) generated by the MSVM block in Figure 11, which are described in Section II.B (see Figure 5(a)), are used to generate the correct pulses. So, the recommended MPC inverter uses the three pulses and the proper M_{dc} value provided by the EV port's current controller to charge the EV batteries. This control method is an advance over its predecessors as it can independently control each of the five MPC inverter ports. This proves that the converter can operate with just two of the four inputs. For instance, if the EV is not connected to the planned MPC inverter, the inverter can utilize the standard sinusoidal pulsewidth modulation (SPWM) method without converting the sinusoidal reference signals into MSVM values. Furthermore, the PV module

could keep working even if the suggested MPC inverter doesn't have an external power source. The current controller of the inverter will modify the dc-link voltage based on the output of the MPPT algorithm, thus maintain the power balance between the PV input and the inverter output. Lastly, the control loops for the battery and SC banks are entirely independent, as shown in Figure 8. So, they may control their power output on their own, regardless of the inverter's modulation method and, by extension, the possible connection to the EV.

EXPERIMENTAL RESULTS

The projected MPC inverter's power circuit and associated control system have been tested in a controlled environment using an experimental prototype. All of the apparatus used in the experiment is shown in Figure 12. The suggested MPC inverter's input ports are shown in Figure 2 connected to a battery and a SCbank, while the EV port is coupled to an extra battery. Figure 2 shows that the PV array is directly connected to the dc connection in line with the specified configuration. Finally, the power circuit output of the proposed MPC inverter was connected via

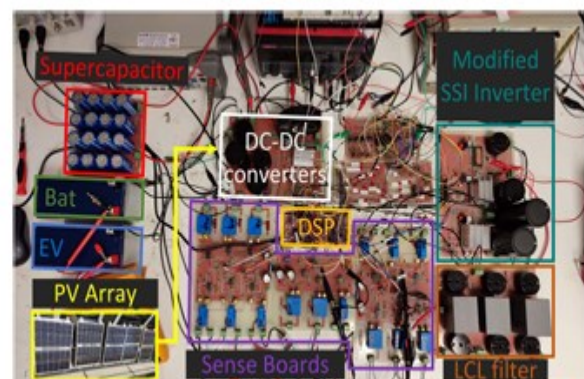


Fig. 12. Experimental prototype of the proposed three-phase grid-connected MPC inverter.

TABLE III. PARAMETERS OF THE EXPERIMENTAL SETUP

Parameter	Description	Value
V_{PV}	Nominal PV array voltage	84 V
V_{SC}	Nominal SC bank voltage	24 V
V_{BAT}	Nominal battery voltage	12 V
V_{EV}	Nominal EV battery voltage	12 V
V_{AC}	Nominal AC grid voltage	230 V rms, 50 Hz
L_{a1}, L_{b1}, L_{c1}	Inverter-side inductance of the LCL-type output filter	4.7 mH
L_{a2}, L_{b2}, L_{c2}	Grid-side inductance of the LCL-type output filter	4.7 mH
C_a, C_b, C_c	Capacitance of the LCL-type output filter	10 μ F
R_D	Damping resistor	5 Ω
$C_{DC-link}$	DC-link capacitance	500 μ F
C_{SC}	SC port capacitance	1000 μ F
C_{BAT}	Battery port capacitance	1000 μ F
C_{EV}	EV port capacitance	1000 μ F
L_{SC}	SC port inductance	4.7 mH
L_{BAT}	Battery port inductance	4.7 mH
L_{EV}	EV port inductance	4.7 mH
f_{SW}	Switching frequency	10 kHz

Connecting the LCL-type output filter to the AC power grid is done for safety reasons after it has passed through a three-phase isolation step-up transformer with a 2:18 turns ratio. The details of the experimental prototype are shown in Table III. The C2000TM LAUNCHXL-F28379D LaunchPad houses the controller, but three IKCM20L60GDXXMA1 intelligent power modules were employed to build the power circuits of the proposed MPC inverter. In Figure 13 and Figure 3(a), respectively, we can see the oscilloscope waveforms of the control (or gate) signals of switches S3 and S1, and the associated voltages VS3 and VS1, respectively. This action represents the emptying of the battery unit and the charging of the SC bank. For the experimental waveforms of the S11 gate signal and the VS11 voltage from Fig. 4(a), refer to Figure 14(a). If you turn off switch S11, the voltage VS11 will be the same as the current passing through its antiparallel diode.

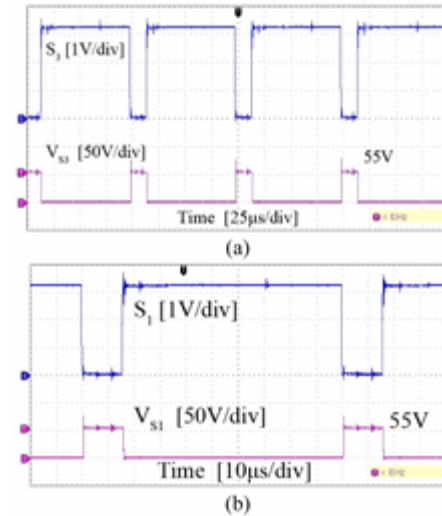


Fig. 13. (a) Gate signal at power switch S3 and voltage VS3. (b) Pulse signal at power switch S1 and voltage VS1

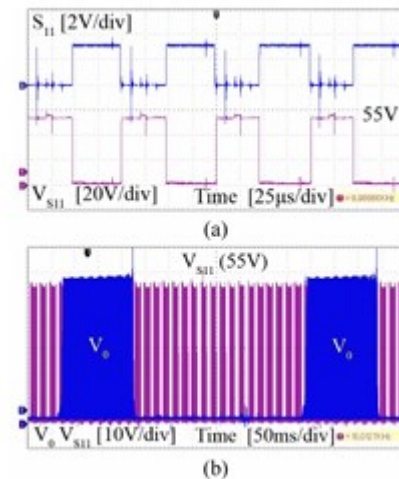


Fig. 14. (a) Gate signal at power switch S11 and voltage VS11. (b) Voltage VO compared with voltage VS11.

as the dc link voltage. Figure 14(b) shows a comparison of the experimental waveforms of the voltages V_O and V_{S11} via simulation. The voltage V_{S11} is determined by switch S11, and the V_O voltage is determined by the three switches S5, S6, and S7 that are connected to the EV connector. We can see that the two voltages don't work at the same frequency; this proves that the three-phase full bridge

switches work at $f_{SW}=10$ kHz and the three EV port switches at 50 Hz. Next, for the purpose of draining the EV battery, the DSP controller set the current setpoint I_{EV} to -1.5 A, as shown in Figure 10. The power switches linked to the EV port work as shown in Figure 15(a), allowing the current I_{EV} to be regulated to the required value, as shown in Figure 15(b)). The battery port works at about 1.5 A when the current setpoint I_{BAT} (refer to Fig. 8) is set to 1.5 A, as seen in the experimental waveforms of Fig. 16A. As shown in Figure 16(b), when the current setpoint I_{SC} is changed to

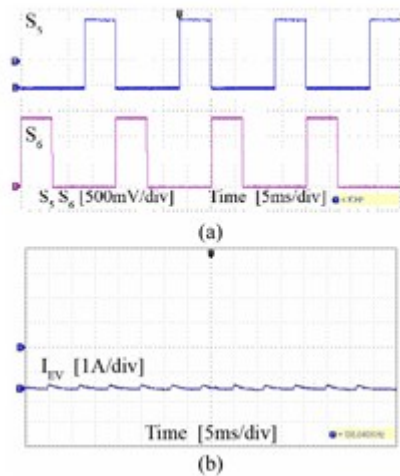


Fig. 15. (a) Gate signals at S5 and S6. (b) Input current at EV port.

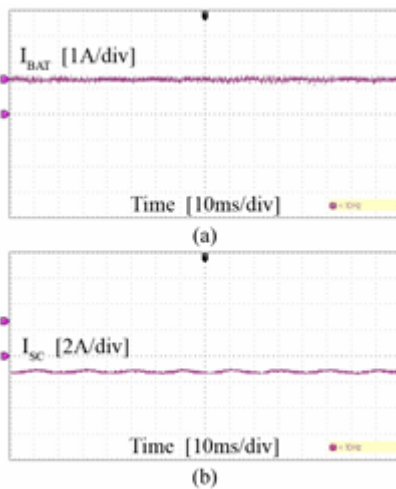
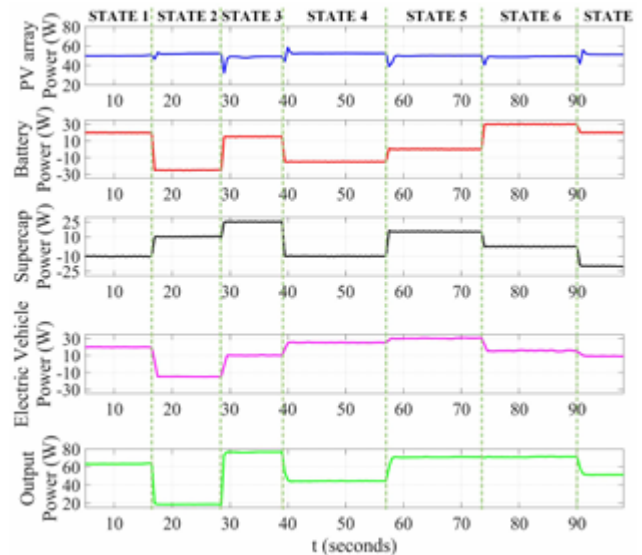


Fig.16.

Experimental results. (a) Input current at battery port. (b) Input current at SC port. TABLE IV EXPERIMENTAL POWER FLOW STATES

State Source	1	2	3	4	5	6	7
P_{PV} (W)	50	50	50	50	50	50	50
P_{BAT} (W)	20	-25	15	-15	0	30	20
P_{EV} (W)	20	-15	10	25	30	15	10
P_{SC} (W)	-10	10	25	-10	15	0	-20

After the DSP-based controller adjusts the A port current to about -1 A, the SC port current is similarly adjusted. These outcomes prove that the power circuit and control technique used by the planned MPC inverter's DSP controller worked as intended. Table IV details the experimental power flow situations used to assess the suggested MPC inverter's performance. You may find the matching outcomes in



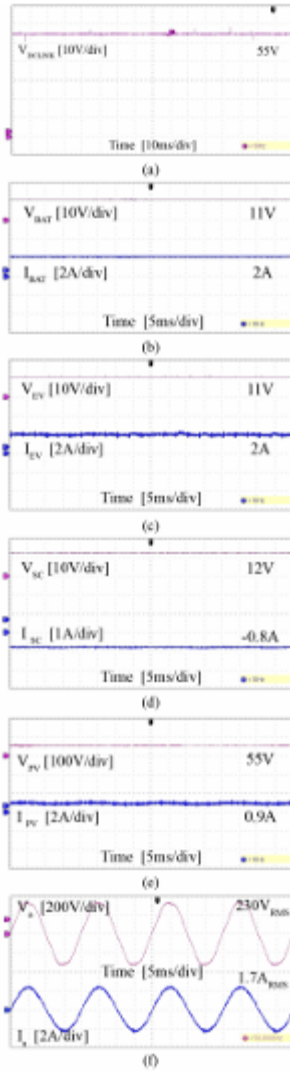


Fig. 18. Experimental measurements at power flow state 1. (a) DC-link voltage. (b) Battery voltage VBAT and current IBAT. (c) EV port voltage VEV and current IEV. (d) SC voltage VSC and current ISC. (e) PV array voltage VPV and current IPV. (f) Electric grid voltage V_{α} of phase a at the secondary of the three-phase protection/isolation step-up transformer and MPC inverter output current I_a of phase a at its primary.

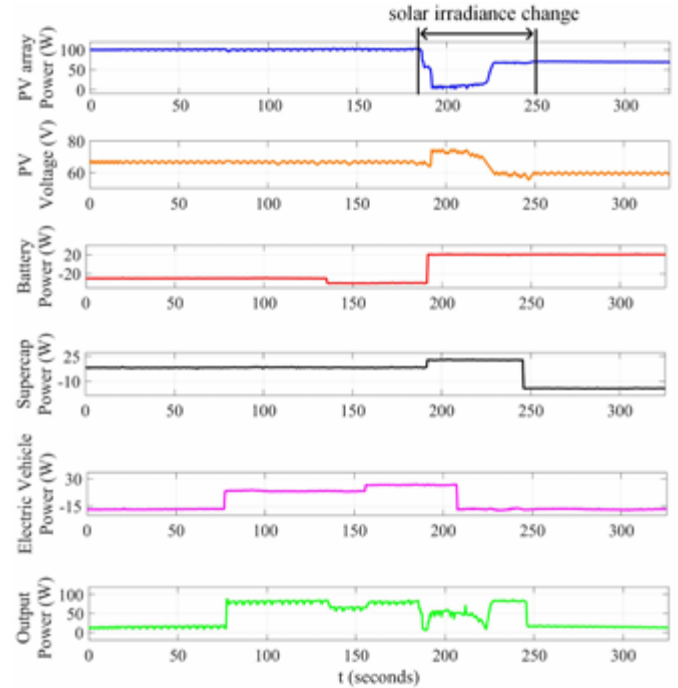
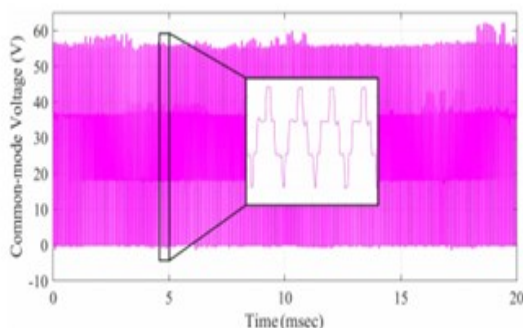


Fig. 19. Experimentally measured power flows and MPPT operation during partial shading conditions.

Scene seventeen. The data shown in Figure 17 indicate that the PV power is stable under all operating circumstances. Experimental power flows were tracked under different operational conditions. The algorithm for PV MPPT was run. As shown in Table IV, the power setpoints for each state are dynamic and accurately followed by the battery, EV port, and SC bank. Fig. 18(a)-(e) displays the pertinent wave forms of the dc-link voltage (VDC-link), currents (I_{PV} , I_{SC} , I_{EV} , and I_{BAT}), and voltages (V_{PV} , V_{SC} , V_{EV} , and V_{BAT}) in the initial condition of the power flow scenarios that were conducted. Figure 18(f) displays the experimental data for the three-phase protection/isolation step-up transformer, including the electric grid voltage (V_{α}) at the secondary of phase a and the MPC inverter output current (I_a) at its primary. The findings demonstrate that the proposed MPC inverter is capable of operating in all power flow scenarios via the independent management of each dc port's current. At the same time as it regulates the power circuit to generate a sinusoidal output current and feed it into the power grid, the controller of the proposed MPC inverter deftly maintains the dc-link voltage at the value indicated by the PV MPPT algorithm. The suggested MPC inverter was tested experimentally under PV array partial

shadowing conditions to guarantee it could independently perform the MPPT process (Fig. 19). Altering the power flows to the battery bank, EV port, and DC was done on purpose using the MPC inverter's DSP-based control unit. The recommended MPC inverters efficiently tracked the PV source's MPPs and separately controlled the power flow to the battery, EV, and SC ports, respectively, to achieve the target levels, even if the MPP power and dc-link voltage are affected by the incident solar irradiance. In the presence of just the PV source, the AC output achieves an efficiency of 96.83%, according to the experiments. However, when the AC output is powered by both the battery and the SC ports, the efficiency drops to 93.14%.



Experimental measurements of the proposed MPC inverter's common-mode voltage (CMV) are shown in Fig. 20. The CMV has an rms value of 32.06 V. The CMV of Figure 20 results in a leakage ground current of 9.3 mA, which meets the requirement of the VDE 0126-1-1 standard, when the PV array has a parasitic capacitance to ground of 100 nF and a ground line impedance of $10 + j\omega \cdot 10^{-5} \Omega$ [22].

CONCLUSION

For the purpose of unifying the interconnection of dispersed RES and hybrid ES systems with the electric grid, this article presents a novel three-phase nonisolated multiport dc-ac power inverter. The power circuit of the proposed MPC inverter allows for a direct connection between the PV source and the dc link, rather of using several dc-dc converters in conjunction with a three-phase full-bridge inverter. In comparison to previous work, the suggested MPC inverter employs less high-frequency power semiconductors and passive components, therefore improving the overall power processing system's dependability. A novel real-time control strategy has been designed with the proposed MPC inverter in

mind. This strategy allows for the following: decoupled control of the modified three-phase SSI subcircuit; adjustment of the ac output power level; regulation of the charging/discharging power of the battery, EV, and SC ports; and the implementation of the MPPT process without the need for an additional power converter. Hence, the suggested MPC inverter may interchange power with the power grid and accomplish integrated power management across four distinct dcports (i.e., PVarray, battery unit, SCbank, and EVbattery). The experimental findings validated that the control strategy and power circuit for the proposed MPC inverter worked well under different power-failure scenarios. Currently, we are working on testing the proposed MPC inverter's potential to provide ancillary services to the electric grid by implementing suitable control algorithms in its control unit.

REFERENCES

- [1]. T. Ariyaratna, N. Kularatna, K. Gunawardane, D. Jayananda, and D. A. Steyn-Ross, "Development of supercapacitor technology and its potential impact on new power converter techniques for renewable energy," *IEEE J. Emerg. Sel. Topics Ind. Electron.*, vol. 2, no. 3, pp. 267–276, Jul. 2021.
- [2]. D. G. A. Krishna, K. Anbalagan, K. K. Prabhakaran, and S. Kumar, "An efficient pseudo-derivative-feedback-based voltage controller for DVR underdistorted grid conditions," *IEEE J. Emerg. Sel. Topics Ind. Electron.*, vol. 2, no. 1, pp. 71–81, Jan. 2021.
- [3]. B. R. Ravada, N. R. Tummuru, and B. N. L. Ande, "A grid-connected converter configuration for the synergy of battery-supercapacitor hybrid storage and renewable energy resources," *IEEE J. Emerg. Sel. Topics Ind. Electron.*, vol. 2, no. 3, pp. 334–342, Jul. 2021.
- [4]. S. Gao, H. Li, J. Jurasz, and R. Dai, "Optimal charging of electric vehicle aggregations participating in energy and ancillary service markets," *IEEE J. Emerg. Sel. Topics Ind. Electron.*, vol. 3, no. 2, pp. 270–278, Apr. 2022.
- [5]. H. Heydari-doostabad and T. O'Donnell, "A wide-range high-voltage-gain bidirectional DC-DC

- converter for V2G and G2V hybrid EV charger," *IEEE Trans. Ind. Electron.*, vol. 69, no. 5, pp. 4718–4729, May 2022.
- [6]. A. Balal and M. Giesselmann, "PV to vehicle, PV to grid, vehicle to grid, and grid to vehicle micro grid system using level three charging station," in *Proc. IEEE Green Technol. Conf.*, 2022, pp. 25–30.
- [7]. W. Jiang and B. Fahimi, "Multiport power electronic interface—Concept, modeling, and design," *IEEE Trans. Power Electron.*, vol. 26, no. 7, pp. 1890–1900, Jul. 2011.
- [8]. P. Shamsi and B. Fahimi, "Dynamic behavior of multi port power electronic interface under source/load disturbances," *IEEE Trans. Ind. Electron.*, vol. 60, no. 10, pp. 4500–4511, Oct. 2013.
- [9]. Z. Ni, A. Abuelnaga, and M. Narimani, "A novel high-performance predictive control formulation for multilevel inverters," *IEEE Trans. Power Electron.*, vol. 35, no. 11, pp. 11533–11543, Nov. 2020.
- [10]. J. Zeng, J. Ning, X. Du, T. Kim, Z. Yang, and V. Winstead, "A four-port DC–DC converter for a standalone wind and solar energy system," *IEEE Trans. Ind. Appl.*, vol. 56, no. 1, pp. 446–454, Jan./Feb. 2020.
- [11]. D. Yu, X. Du, J. Zeng, and Z. Yang, "Control of a grid-tied multiport inverter for a microgrid with renewable energy sources," in *Proc. IEEE Energy Convers. Congr. Expo.*, 2020, pp. 2467–2471.
- [12]. S. A. Khan, M. R. Islam, Y. Guo, and J. Zhu, "A new isolated multi-port converter with multi-directional power flow capabilities for smart electric vehicle charging stations," *IEEE Trans. Appl. Supercond.*, vol. 29, no. 2, Mar. 2019, Art. no. 0602504.
- [13]. S. Neira, J. Pereda, and F. Rojas, "Three-port full-bridge bidirectional converter for hybrid DC/DC/AC systems," *IEEE Trans. Power Electron.*, vol. 35, no. 12, pp. 13077–13084, Dec. 2020.
- [14]. A. M. Haddadi, S. Farhangi, and F. Blaabjerg, "A reliable three-phase single-stage multiport inverter for grid-connected photovoltaic applications," *IEEE J. Emerg. Sel. Topics Power Electron.*, vol. 7, no. 4, pp. 2384–2393, Dec. 2019.
- [15]. H. Wu, L. Zhu, and F. Yang, "Three-port-converter-based single-phase bidirectional AC–DC converter with reduced power processing stages and improved overall efficiency," *IEEE Trans. Power Electron.*, vol. 33, no. 12, pp. 10021–10026, Dec. 2018.
- [16]. A. Abdelhakim, P. Mattavelli, and G. Spiazzi, "Three-phase split-source inverter (SSI): Analysis and modulation," *IEEE Trans. Power Electron.*, vol. 31, no. 11, pp. 7451–7461, Nov. 2016.
- [17]. A. Abdelhakim, P. Mattavelli, V. Boscaino, and G. Lullo, "Decoupled control scheme of grid-connected split-source inverters," *IEEE Trans. Ind. Electron.*, vol. 64, no. 8, pp. 6202–6211, Aug. 2017.
- [18]. S. S. Lee and Y. E. Heng, "Improved single-phasesplit-source inverter with hybrid quasi-sinusoidal and constant PWM," *IEEE Trans. Ind. Electron.*, vol. 64, no. 3, pp. 2024–2031, Mar. 2017.
- [19]. V. M. R. de Jesus, A. F. Cupertino, L. S. Xavier, H. A. Pereira, and V. F. Mendes, "Comparison of MPPT strategies in three-phase photovoltaic inverters applied for harmonic compensation," *IEEE Trans. Ind. Appl.*, vol. 55, no. 5, pp. 5141–5152, Sep./Oct. 2019.
- [20]. F. Blaabjerg, R. Teodorescu, M. Liserre, and A. V. Timbus, "Overview of control and grid synchronization for distributed power generation systems," *IEEE Trans. Ind. Electron.*, vol. 53, no. 5, pp. 1398–1409, Oct. 2006.